THE ASTROPHYSICAL JOURNAL, **181**: 781–794, 1973 May 1

INTERFEROMETRIC OBSERVATIONS OF FORMALDEHYDE ABSORPTION IN FRONT OF STRONG GALACTIC SOURCES

E. B. FOMALONT
National Radio Astronomy Observatory,* Green Bank, West Virginia
AND
L. WELIACHEW†
California Institute of Technology, Owens Valley Radio Observatory
Received 1972 August 18; revised 1972 December 4

ABSTRACT

Observations have been made of formaldehyde absorption at 4830 MHz in front of Sgr A, Sgr B2, W3, NGC 2024, W31, W33, W43, W49A, and W51. The Caltech interferometer, consisting of two 90-foot paraboloids, was used to synthesize a beam of $40'' \times 60'' \sec(\delta - l)$, where δ is the source declination and $l = 38°$. The main absorption features show variations of optical depth over the sources, but there is no significant clumping.

The previously determined isotopic ratio $^{12}C/^{13}C$ of 10 for Sgr A and Sgr B2 should be increased to $\sim 25 \pm 5$ for Sgr A and ≥ 20 for Sgr B2 because of the high optical depths at the center of the absorbing clouds, $\tau_{max} \sim 2.0$ for Sgr A, $\tau_{max} \gtrsim 3$ for Sgr B2.

The $+40$ km s^{-1} cloud associated with Sgr A appears to be rotating as a solid body. The mass of the cloud is calculated to be $\sim 3 \times 10^5 M_\odot$. From neutral-hydrogen absorption data only a small proportion of the cloud is composed of atomic hydrogen; hence the cloud consists mainly of molecular hydrogen with a density $\sim 10^5$ cm^{-3}.

Subject headings: abundances, nebular — molecules — nebulae — radio sources

I. INTRODUCTION

Interferometric observations of the 4830-MHz formaldehyde absorption in front of nine strong galactic sources have been made with a resolution of $40'' \times 60'' \sec(\delta - l)$. The main purpose was to obtain an approximate size of the absorbing clouds. A uniform absorption over a source would imply that the clouds are much larger than the source (typically 4′), whereas clouds smaller than 4′ could be resolved by our data. In particular, we wished to determine if the surprisingly low isotopic abundance ratio of $^{12}C/^{13}C \approx 10$ found in the absorption associated with Sgr A and Sgr B2 (Zuckerman *et al.* 1969) might be due to a high optical depth in $H_2{}^{12}CO$ from part of the cloud. Only the strongest absorption feature associated with each source has been synthesized. These clouds are probably associated with the radio source and may not be representative of all clouds with formaldehyde absorption (Whiteoak and Gardner 1970).

II. OBSERVATIONS AND REDUCTION

The observations were made in 1970 with the Owens Valley Radio Interferometer consisting of two movable 90-foot (27-m) antennas. The source list included Sgr A, Sgr B2, W3, NGC 2024, W31, W33, W43, W49A (the thermal component of W49), and W51, all of which are strong continuum sources at 4830 MHz, significantly

* Operated by Associated Universities, Inc., under contract with the National Science Foundation.

† Permanent address: Departement de Radioastronomie, Observatoire de Meudon, 92-Meudon, France.

absorbed by formaldehyde, and not too large in angular size ($\leq 4'$). Each antenna was equipped with a 6-cm parametric amplifier of noise temperature 150°. An image rejection filter was used to suppress the lower sideband of the heterodyne receiver. The receiving system that was used is similar to the single-channel system described by Read (1963). For line work the intermediate-frequency signals from the two antennas were fed into two similar sets of narrow-band filters and the outputs from each corresponding pair of filters were then multiplied to give the usual fringes. For Sgr A and Sgr B2, 23–100 kHz filters were used. For the remaining sources 23–50 kHz filters were sufficient to cover the important absorption lines. The continuum channel with a bandwidth of 5 MHz was also recorded.

The duration of an observation was 15 minutes with a resultant rms fluctuation of 0.2 and 0.3 flux units for the 100- and 50-kHz channels, respectively. The local oscillator was controlled by a frequency synthesizer to center the absorption feature in the bandpass and compensate for the Earth orbital and diurnal motion as well as for the solar motion toward the local standard of rest. The antennas were sensitive to linear polarization with the electric vector aligned in position angle 0°.

The spacings used were 100, 200, 400, and 600 feet east-west and 400 feet north-south. One hundred feet corresponds to 500 wavelengths which gives a 6.6 fringe. Most sources were observed over the range -4^h to $+4^h$ hour angle to give a reasonable coverage in resolution. The approximate synthesized beam width is 40″ east/west by 60″ sec ($\delta - l$) north/south. The grating response was about 6′ in the east-west direction and ~ 3.5 sec ($\delta - l$) in the north-south direction. Structure as large as or larger than the grating response was resolved out.

The gain variations, phase changes, and baseline error of the system were calibrated using small-diameter sources of known strength and position (Fomalont, Wyndham, and Bartlett 1967). These corrections can be determined from the broad-band channel. In addition, there is a slow drift in gain and phase between the broad band and each narrow band which was determined by observing a strong source (to give sufficient signal to noise in the narrow bands) a few times a day (Rogstad, Rougoor, and Whiteoak 1967).

III. INVERSION OF THE DATA

The optical depth and projected density of the formaldehyde over the sources were determined as follows. For each 15-minute observation the complex visibility function for the continuum $V_C(u, v)$ and the complex visibility function for each narrow band $V_{NB}(u, v)$, where u is the projected east-west spacing and v is the projected north-south spacing, were determined. The continuum visibility function was derived from the continuum channel (which was 5 MHz in bandwidth so that only a negligible fraction of power across the band was absorbed by formaldehyde) or from an average of the unabsorbed narrow bands for some sources. The difference $\Delta V_{NB}(u, v) = V_C(u, v) - V_{NB}(u, v)$ is the visibility function of the absorption in a narrow band. Taking the Fourier transforms gives

$$V_C(u, v)(\text{F.T.}) \rightarrow T_C(x, y)\,, \tag{1}$$

$$\Delta V_{NB}(u, v)(\text{F.T.}) \rightarrow A_{NB}(x, y)\,, \tag{2}$$

where $T_C(x, y)$ is the brightness distribution of the continuum and $A_{NB}(x, y)$ the brightness distribution of the absorbed intensity for each narrow band. From the ratio of A_{NB} to T_C the distribution of optical depth $\tau_{NB}(x, y)$ could be determined:

$$\frac{A_{NB}(x, y)}{T_C(x, y)} = 1 - \exp\left[-\tau_{NB}(x, y)\right]. \tag{3}$$

Integrating over all narrow bands

$$NLT^{-1}(x, y) \sim \Delta\nu \sum_{\mathrm{NB}} \tau_{\mathrm{NB}}(x, y) \tag{4}$$

gives the quantity NLT^{-1} over the source, where NL is the projected density of the H_2CO molecules in cm^{-2}, T the excitation temperature (° K) of the line, and $\Delta\nu$(Hz) is the bandwidth of each narrow band. The conversion of $\Delta\nu \sum \tau$ into a projected density of H_2CO molecules has been made following the assumptions of Zuckerman *et al.* (1970*a*, hereinafter quoted as ZBPS).

Because the data did not provide a complete aperture synthesis of the source, normal Fourier inversion techniques were not the most useful method to determine the brightness distribution from the visibility functions. A model brightness distribution composed of several Gaussian-shaped components was first chosen from inspection of the visibility function. An iterative technique then varied the parameters of the model to fit the observations within the experimental errors (Fomalont 1968). The results were cross-checked by a Fourier-inversion scheme developed by Högbom (private communication). There is good agreement in the sense that slight differences in the two methods do not affect the conclusions of the paper. For the source W3, observations were sufficiently detailed and only a Fourier inversion was used.

An accurate estimate of the inversion errors due to noise and incomplete aperture sampling is difficult to obtain. Unless otherwise specified, the inversion error is approximately equal to one-half contour interval.

IV. RESULTS

The resulting continuum and projected densities for W3, NGC 2024, W31, W43, and W49A are shown in figures 1–5. Some variation of the absorption distribution with velocity was noticed for these sources, but these differences were not much larger than the expected variation due to noise. On the left is the brightness distributions at 4830 MHz of the continuum radiation determined from the continuum channel. The coordinates are given at epoch 1950.0, and the synthesized half-power beamwidth is shown by the crosshatched area. Ten percent contour levels are drawn. To the right, the projected density NLT^{-1} of the formaldehyde absorption, using the method outlined in the previous section, is shown by the contours. All narrow-band channels with

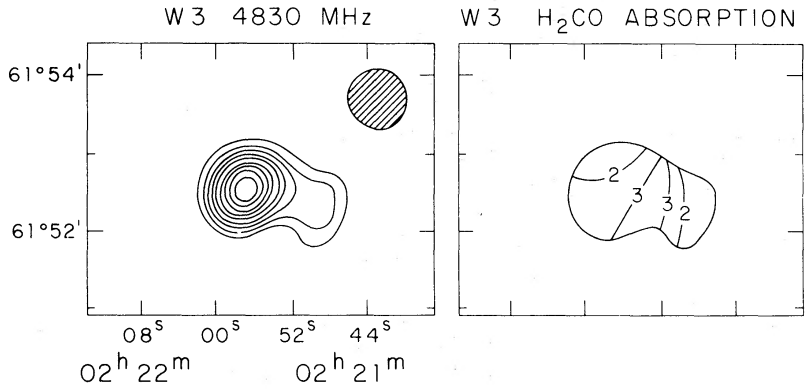

FIG. 1*a* (*left*).—Continuum brightness distribution for W3. Peak brightness temperature is 830° K with 10 percent contour levels. Synthesized beam shown by crosshatched area. FIG. 1*b* (*right*).—Distribution of NLT^{-1} for -41 km s^{-1} line of W3. Contour unit = 0.40×10^{13} cm^{-2} (deg-K)$^{-1}$, and the outer boundary is 10 percent continuum contour. The velocity range of -39.7 to -42.8 km s^{-1} was used.

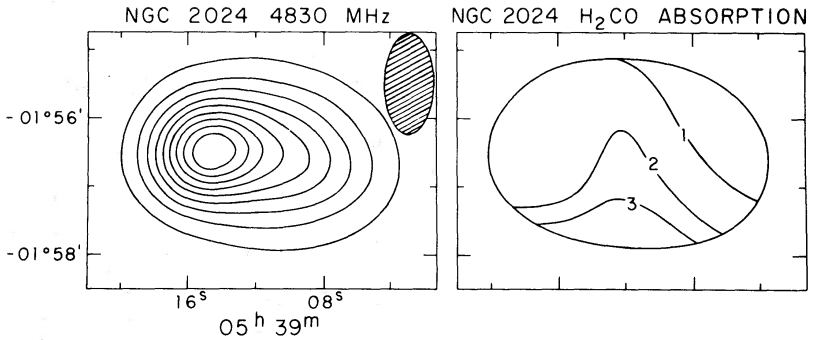

FIG. 2*a* (*left*).—Continuum brightness distribution for NGC 2024. Peak brightness temperature is 190° K with 10 percent contour levels. Synthesized beam shown by crosshatched area. FIG. 2*b* (*right*).—Distribution of NLT^{-1} for +8.65 km s^{-1} line of NGC 2024. Contour unit = 0.88 × 10^{13} cm^{-2} (deg-K)$^{-1}$, and the outer boundary is 10 percent continuum contour. The velocity range of 7.1 to 10.2 km s^{-1} was used.

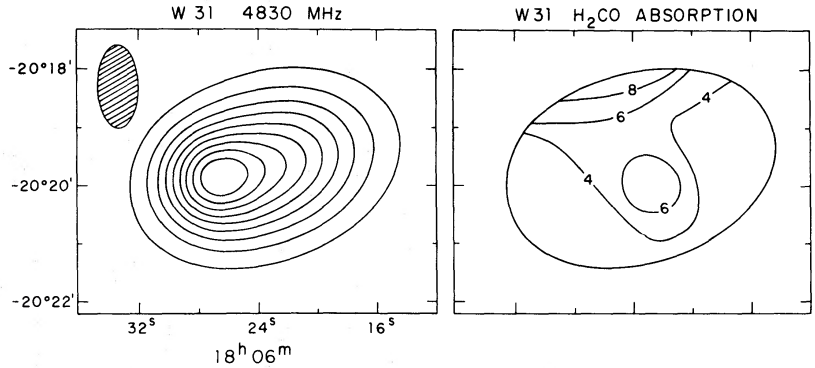

FIG. 3*a* (*left*).—Continuum brightness distribution for W31. Peak brightness temperature is 192° K with 10 percent contour levels. Synthesized beam is shown by crosshatched area. FIG. 3*b* (*right*).—Distribution of NLT^{-1} for +9.8 km s^{-1} line of W31. Contour unit = 0.88 × 10^{13} cm^{-2} (deg-K)$^{-1}$, and the outer boundary is 10 percent continuum contour. The velocity range of −4.5 to 20.7 km s^{-1} was used. There is a blend of two clouds in the range according to ZBPS.

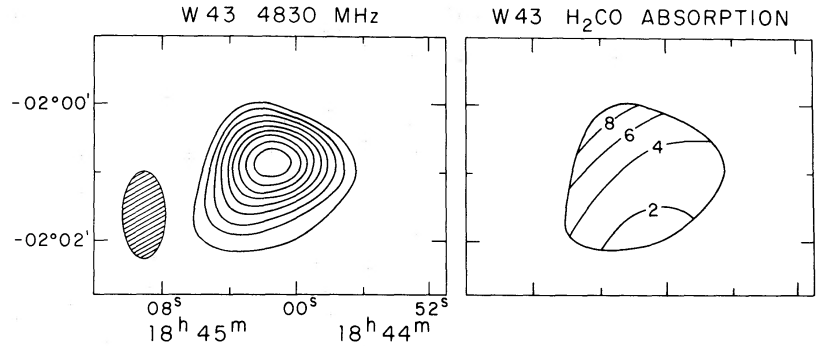

FIG. 4*a* (*left*).—Continuum brightness distribution for W43. Peak brightness temperature is 195° K with 10 percent contour levels. Synthesized beam is shown by crosshatched area. FIG. 4*b* (*right*).—Distribution of NLT^{-1} for +91.2 km s^{-1} line of W43. Contour unit = 0.88 × 10^{13} cm^{-2} (deg-K)$^{-1}$, and the outer boundary is 10 percent continuum contour. The velocity range of 86.5 to 99.0 km s^{-1} was used.

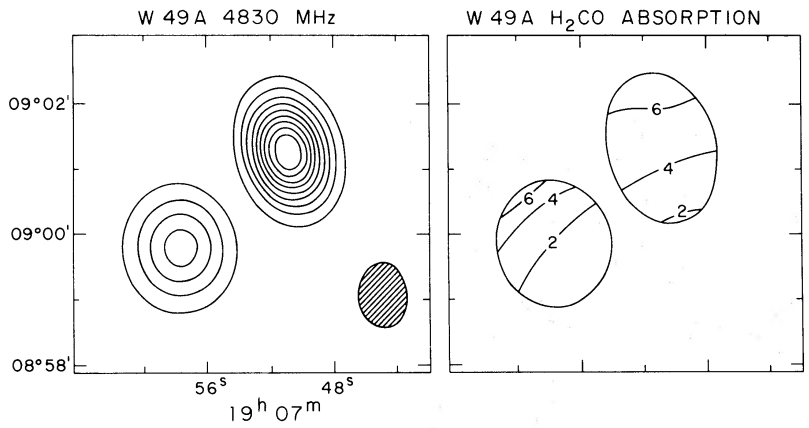

FIG. 5*a* (*left*).—Continuum brightness distribution for W49A. Peak brightness temperature is 230° K with 10 percent contour levels. Synthesized beam is shown by crosshatched area. FIG. 5*b* (*right*).—Distribution of NLT^{-1} for +13.8 km s^{-1} line of W49. Contour unit = 0.88 × 10^{13} cm^{-2} (deg-K)$^{-1}$, and the outer boundary is 10 percent continuum contour. The velocity range 6.0 to 21.1 km s^{-1} was used.

significant absorption in the main absorption feature have been used to obtain the maps. The 10 percent contour from the continuum map has been taken as the outer boundary of the absorption map. The errors of the optical depth are too large for a meaningful distribution outside of this limit. No corrections have been made for the primary beam which has a half-power beamwidth of 9′.

For W51, Sgr A, and Sgr B2 significant variation of the absorption over the velocity range of the main feature was obtained. The result for W51 is shown in figure 6; the continuum radiation (*left*), the projected density of formaldehyde absorption between 54.6 and 60.7 km s^{-1} (*right*), and between 60.7 and 70.0 km s^{-1} (*middle*). The difference is consistent with the spectrum given by ZBPS, who suggest a blend of two features at ~58 and ~65 km s^{-1}, and the CO observations of Penzias *et al.* (1971) who noted two separate features at 57 and 70 km s^{-1}, the latter being to the southwest of the continuum.

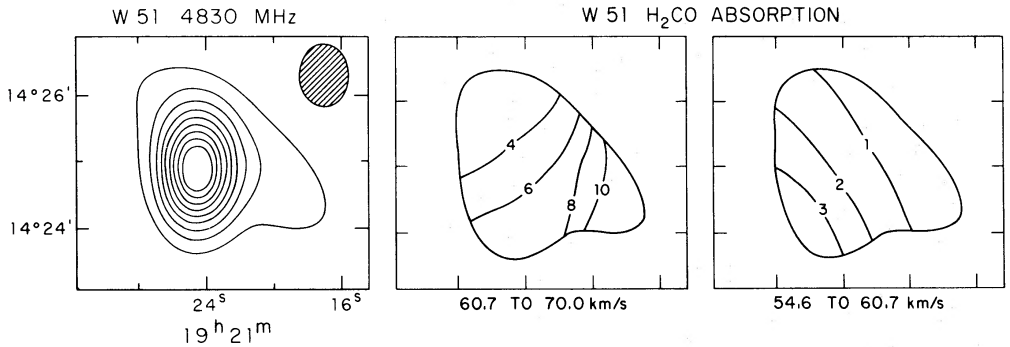

FIG. 6*a* (*left*).—Continuum brightness distribution of W51. Peak brightness temperature is 460° K with 10 percent contour levels. Synthesized beam is shown by crosshatched area. FIG. 6*b* (*middle*).—Distribution of NLT^{-1} for ~65 km s^{-1} line of W51. Contour unit = 0.88 × 10^{13} cm^{-2} (deg-K)$^{-1}$, and the outer boundary is 10 percent continuum contour. The velocity range 60.7 to 70.0 km s^{-1} was used. FIG. 6*c* (*right*).—Distribution of NLT^{-1} for ~58 km s^{-1} line of W51. Contour unit = 0.88 × 10^{13} cm^{-2} (deg-K)$^{-1}$. The velocity range 54.6–60.7 km s^{-1} was used.

The results for Sgr B2 are given in figures 7 and 8. Figure 7 shows the continuum distribution and the projected density of formaldehyde absorption from the main feature, and figure 8 shows the distribution of optical depth across Sgr B2 for the various 100-kHz narrow-band channels within the main absorption feature. The 10 percent continuum level has been taken as the outer boundary.

The continuum distribution for Sgr A is given in figure 9. The contour levels are 10 percent except for the outer contour of 5 percent. The distribution of optical depth across Sgr A (within the 5 percent continuum contour) for various 100-kHz narrow band channels between 22.6 and 66.0 km s^{-1} are shown in figure 10. The absorption at radial velocities less than 25 km s^{-1} pertains to a feature separate from that centered around 40 km s^{-1}. The absorption that is seen at these lower velocities is produced in an unrelated cloud to the north of the continuum peak. There is not sufficient continuum radiation to observe H_2CO absorption at the position of NH_3 and 2-mm H_2CO emission detected to the south of the source at velocities ~ 20 km s^{-1}.

The projected density of the formaldehyde from the entire "40 km s^{-1}" feature is displayed in figure 11. Only velocities between 29 and 66 km s^{-1} are included, and the approximate distribution of the velocity field of the cloud is shown by the dashed lines. Positional data from other observations are also shown; data for NH_3 emission from Cheung *et al.* (1968), 2-mm formaldehyde emission from Thaddeus *et al.* (1971), and the occultation data of Kerr and Sandquist (1968, 1970) are used for OH and H_2CO absorption. Emission from CO (Penzias, Jefferts, and Wilson 1971) is widespread but appears to have a maximum near the absorption peak.

A summary of the derived values of NLT^{-1} for each source is given in table 1. The radial velocity of the line center and line width have been taken from ZBPS, except for Sgr A which we have slightly modified to exclude the absorption below +29 km s^{-1}. Three values of NLT^{-1} integrated over each source are given in table 1. The first value is taken from ZBPS who assumed uniform coverage of the absorption. The second value was derived from maps obtained by a Fourier inversion scheme of the data, and the third value was obtained from a model fit of the data. Both methods were described in § III. The total continuum flux density measured at a spacing of 100 feet E/W is given in the last column. For NGC 2024 and W43 the 100-foot E/W flux

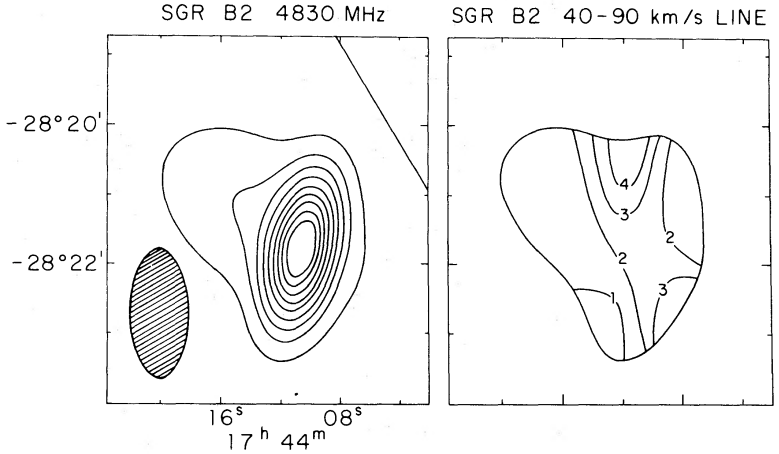

FIG. 7*a* (*left*).—Continuum brightness distribution for Sgr B2. Peak brightness temperature is 310° K with 10 percent contour levels. Synthesized beam is shown by crosshatched area. The galactic equator is shown by the line in the upper right corner. FIG. 7*b* (*right*).—Distribution of NLT^{-1} for +61.6 km s^{-1} line of Sgr. B2. Contour unit = 44×10^{13} cm^{-2} $(deg\text{-}K)^{-1}$, and the outer boundary is 10 percent continuum contour. The velocity range 40.0–89.2 km s^{-1} was used.

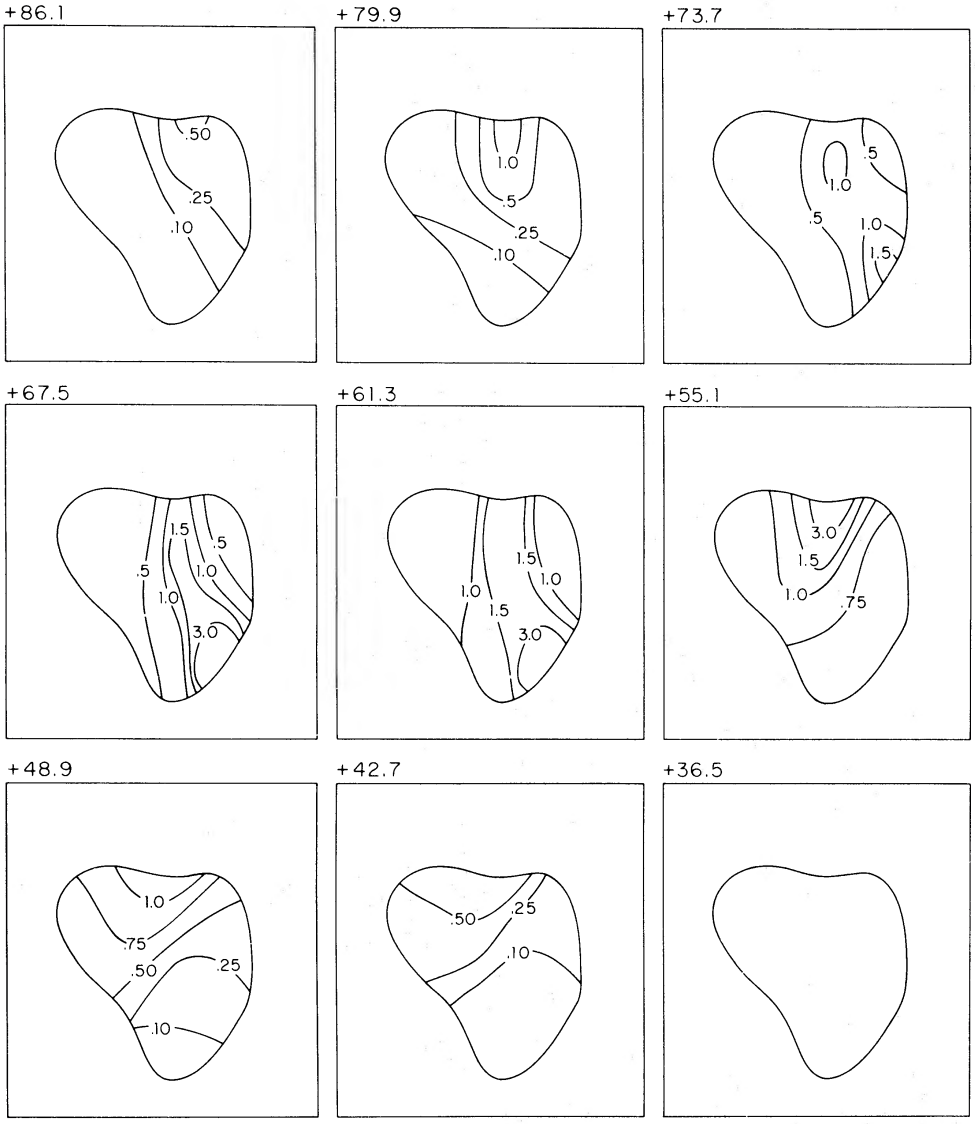

FIG. 8.—Optical depth of formaldehyde absorption in Sgr B2. The contour levels for each plot give the optical depth. The radial velocity with respect to the LSR for the center of each channel is shown above each plot. The velocity width of each channel is 6.2 km s^{-1}. The 10 percent continuum contour has been taken as the outer boundary of the maps, and the scale of each map can be derived from fig. 7. Because of a 5 percent error in the formaldehyde absorption intensity, a region of opacity larger than 3.0 could have an infinite optical depth.

density is significantly less than the flux density observed with the 140′ antenna by ZBPS. This is caused by the resolution of the large-scale continuum by the interferometric observations. The agreement of NLT^{-1} with ZBPS suggests that the optical depth does not change significantly across the whole continuum source.

The agreement between the model fit value and the Fourier inversion value of NLT^{-1} is good. Except for Sgr A and Sgr B2 these values also agree with those of ZBPS. The differences for Sgr A and Sgr B2 are due to the large optical depth of the formaldehyde cloud over each source.

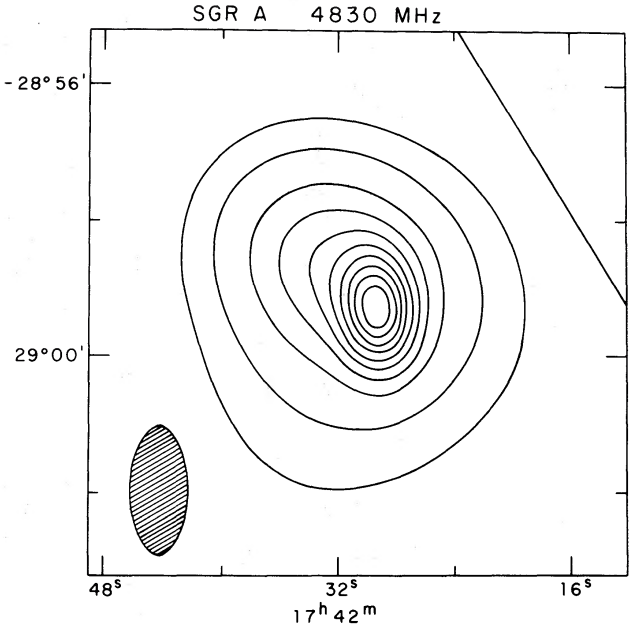

FIG. 9.—Continuum brightness distribution for Sgr A. Peak brightness temperature is 445° K. Ten percent contours are drawn with the outer contour at 5 percent. The synthesized beam is given by the crosshatched area and the galactic equator is shown by the line in the upper right corner.

TABLE 1

PROJECTED DENSITY OF FORMALDEHYDE ABSORPTION

SOURCE	GALACTIC COMPONENT	RADIAL VELOCITY* (km s^{-1})	ΔV† (km s^{-1})	NLT^{-1} ($\times 10^{-13}$) ZBPS‡	FI‡	MF‡	FLUX DENSITY§
Sgr A.....	G0.0−0.1	+46	32	10.1	18	25.4	146
Sgr B2.....	G0.7−0.1	+61.6	26.3	59	>124‖	>98‖	39
W3.....	G133.7+1.2	−41.1	2.8	1.1	0.9	...	42
NGC 2024...	G206.5−16.4	+ 8.65	1.5	1.0	1.6	1.3	32
W31.....	G10.2−0.3	+ 9.8	9.2	3.5	4.7	4.0	46
W33#	G12.8−0.2	+34.0	5.5	...	...	7.8	19.4
W43.....	G30.8−0.0	+91.2	7.3	3.7	3.4	4.0	28.3
W49A.....	G43.2+0.0	+13.8	7.6	3.2	3.5	3.1	33
W51.....	G49.5−0.4	+65.4	7.8	5.4	4.2	6.9	70

* Velocities are with respect to the local standard of rest and taken from ZBPS except for Sgr A.

† Line widths taken from ZBPS except for Sgr A.

‡ ZBPS = projected density determined by ZBPS assuming uniform coverage, FI = Fourier inversion, MF = model fit of present data.

§ Total flux density in flux units measured for continuum source.

‖ Assumes maximum opacity of 3.0.

Only a small diameter component ~20″ was observed. Cannot be compared with ZBPS which included nearby large diameter components.

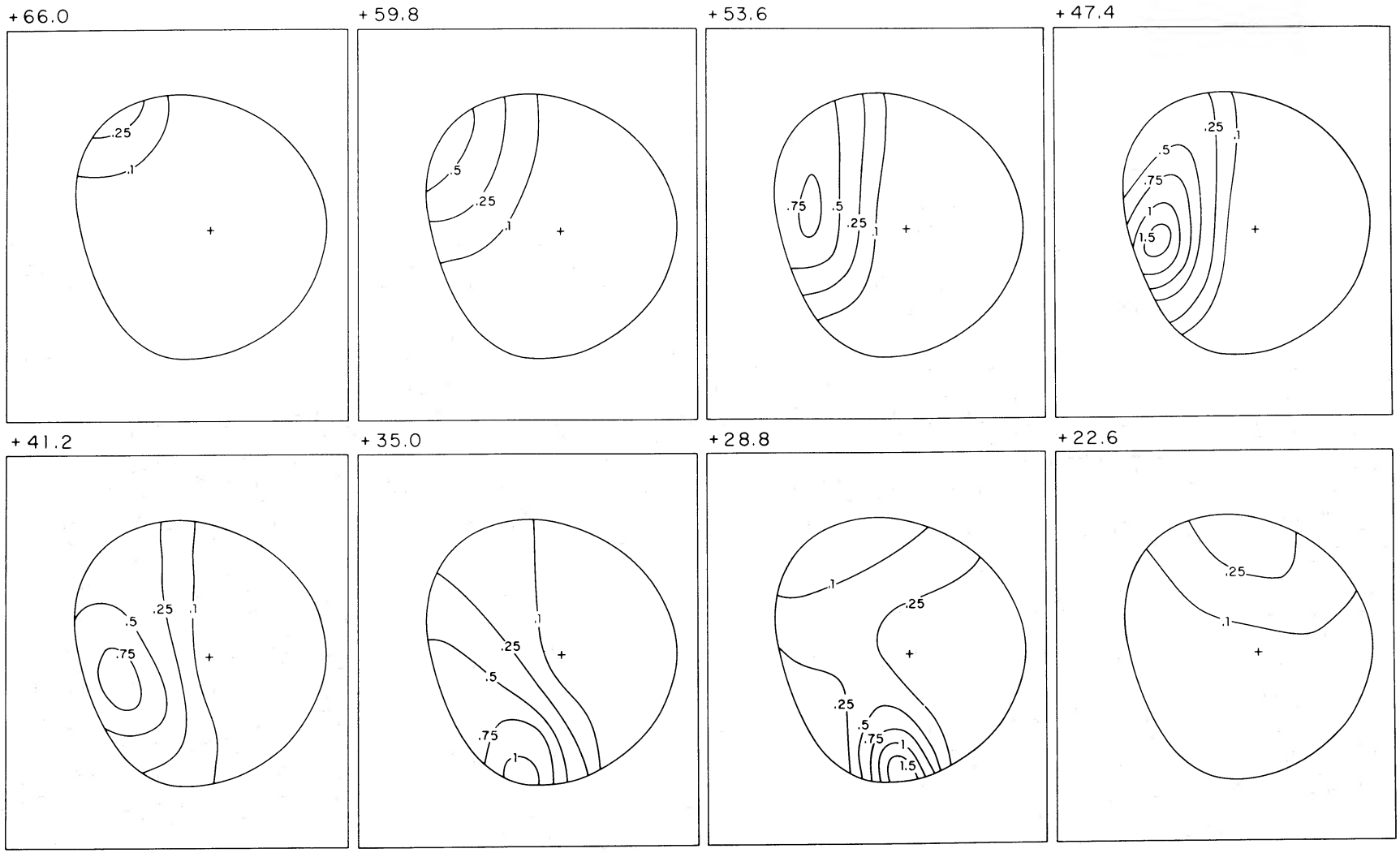

FIG. 10.—Optical depth of formaldehyde absorption in Sgr A. The radial velocity with respect to the LSR for the center of the channel is shown above each plot. The continuum peak is shown by the cross. The 5 percent continuum contour has been taken as the outer boundary of the maps, and the scale of each map can be derived from fig. 9.

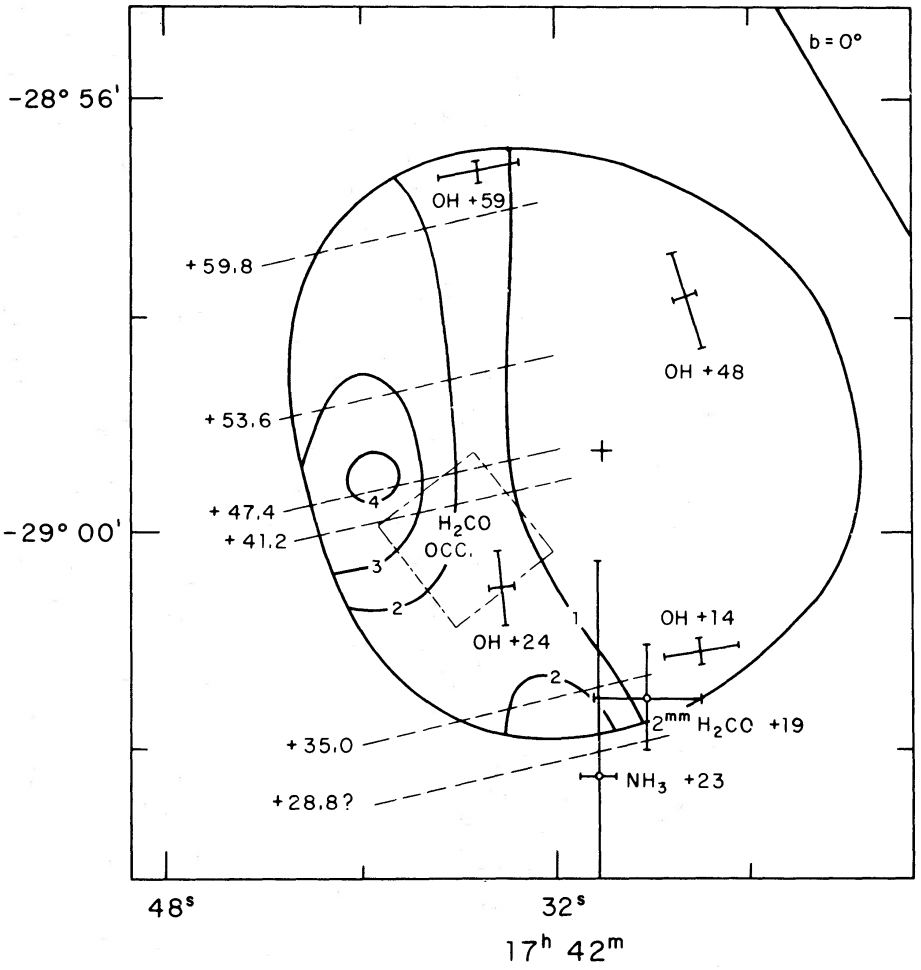

FIG. 11.—Distribution of NLT^{-1} for +40 km s^{-1} line of Sgr A. The contour levels are 17.6 × 10^{13} cm^{-2} (deg-K)$^{-1}$. The galactic equator is given by the line at the upper right. The dashed lines give the velocity field. The positional and velocity data for other atoms and molecules are given in the plot (see text).

V. DISCUSSION

a) Cloud Size

From figures 1–7 it appears that the clouds are about the same size as the sources they absorb. None of the sources are uniformly absorbed but show a simple variation consistent with one cloud except for W51 and possibly W31. With the present resolution there is typically a range of three to one in the projected density of formaldehyde across the source. Small clouds of the order of 1′ in size which could have been detected are not present. Only in Sgr A has a cloud been isolated, but its size is comparable to the source. It is, of course, possible that the clouds are composed of many small clumps each smaller than the synthesized beam. Since we have not observed the $H_2{}^{13}CO$ profile, we are not able to compare the ^{12}C and ^{13}C profiles for an indication of further clumpiness (ZBPS; Gardner and Whiteoak 1971).

b) Physical Conditions in the Clouds

Table 2 shows estimates of the upper limits of H_2CO for all of the sources (Sgr A will be considered separately). The estimates were made from the values NLT^{-1} listed in column (7) of table 1 except for W3 where the Fourier inversion solution was taken. The distance to the cloud given in column (2) has been taken as equal to the distance of the source for all cases. Since each cloud covers the entire source, we have taken the source angular size as the lower limit to the cloud angular size and further assumed a line-of-sight length L of the cloud equal to its transverse dimension. Thus the derived densities are probably upper limits to the average densities. They do not exclude much larger densities in restricted regions. We have adopted an excitation temperature of 3° K for the 6-cm formaldehyde transition. The corresponding upper limits to the volume density of H_2 molecules are also given in table 2. We have assumed a ratio of N_{H_2CO} to N_{H_2} of 2×10^{-9}, the approximate value derived from Orion A by Thaddeus *et al.* (1971).

The assumption concerning the distance to the clouds is justified by the following conditions. Except Sgr A, all of the continuum sources are thermal and show radio recombination lines of hydrogen (Reifenstein *et al.* 1970). For all sources where ZBPS detected several H_2CO features, the feature with the largest value of NLT^{-1} is the closest in velocity to the H109α line velocity. Hence, the most important contribution to the formaldehyde absorption comes from a feature associated with the H II feature. As already mentioned, the observations reported here were only devoted to these strong features in absorption.

The other weaker features detected by ZBPS are probably similar to the "anomalous" absorption features detected in dark nebulae by Palmer *et al.* (1969). The anomalous absorption features also have narrower line widths. Among 57 absorption features detected (Snyder 1971, private communication), 47 have line widths less than 2 km s^{-1}, and only two have widths greater than 4 km s^{-1}. On the other hand the H_2CO features associated with H II regions generally show much larger line widths. Whiteoak and Gardner (1970) also noted a statistical trend in which the clouds of high optical depth have velocities near the H II velocity.

An excitation temperature of 3° K due to the microwave background for the 6-cm transition cannot be justified in a rigorous manner. However, the following points should be made. First, the excitation temperature of the transition is unlikely to be as large as the kinetic temperature of 10°–20° K for the clouds deduced from the CO

TABLE 2

UPPER LIMITS OF H_2CO AND H_2 DENSITIES

Source	D* (kpc)	Standard† Size (arc min)	Adopted NLT^{-1} (10^{13} cm^{-2} ° K^{-1})	n_{H_2CO} (cm^{-3})	n_{H_2} (cm^{-3})
Sgr B2.....	10	2.2	98	148×10^{-6}	74×10^{3}
W3.....	3.1	1.4	0.9	6.9×10^{-6}	3.4×10^{3}
NGC 2024.....	0.6	2.9	1.3	2.5×10^{-6}	1.2×10^{3}
W31.....	13‡	3	4.0	3.4×10^{-6}	1.7×10^{3}
W43.....	7	2	4.0	9.5×10^{-6}	4.7×10^{3}
W49A.....	14	4	3.1	1.8×10^{-6}	0.9×10^{3}
W51.....	7	2	6.9	16×10^{-6}	8×10^{3}

* All distances except W31 are from Reifenstein *et al.* (1970).

† Lower limit on H_2CO cloud size.

‡ Average between several estimates ranging from 9 to 17 kpc.

emission. Of the eight thermal sources listed in table 1, five have CO emission (Penzias *et al.* 1971). This emission occurs at a velocity close to the recombination-line and H_2CO line velocities; hence, it is likely that the CO emission is coextensive with the H_2CO absorption. Penzias *et al.* show that the kinetic temperature of these clouds is in the range 10°–20° K. But coupling of the H_2CO excitation temperature to the kinetic temperature requires $N_{H_2} \gtrsim 2 \times 10^5$ cm^{-3}. Such densities are likely to be found only in some particularly dense regions. This is shown by the detection of 2-mm H_2CO emission only from very restricted regions in W3(OH), Sgr A, W51, and Orion. In addition, Thaddeus *et al.* (1971) showed that electron densities are always too low to couple the excitation temperature to the kinetic temperature.

Second, the cooling mechanism needed by Palmer *et al.* (1969) to explain the apparent absorption of the microwave background by the dark nebulae may not be operative in the clouds studied here which are probably associated with thermal sources. Theoretical arguments concerning the cooling mechanism (see, e.g., Townes and Cheung 1969; White 1971; Thaddeus 1972) are still conflicting. Also, the lack of detected emission from the clouds observed here yield irrelevant lower limits on the excitation temperature. Hence 3° K is adopted as the excitation temperature.

c) $^{12}C/^{13}C$ *Ratio*

The apparent $^{12}C/^{13}C$ isotropic ratio (Zuckerman *et al.* 1969) of ~ 10 for Sgr A and Sgr B2 should be revised upward. From table 1 the value of NLT^{-1} for both sources are a factor 2 or 3 times larger than that found by ZBPS who assumed uniform coverage in deriving their number. The large optical depth of the $H_2{}^{12}CO$ species near the center frequency of the line is shown in figure 8 for Sgr B2 and figure 10 for Sgr A. For the sources in table 1 outside the galactic center, there is good agreement with ZBPS for the values of NLT^{-1}. Thus a $^{12}C/^{13}C$ isotopic ratio derived at low resolution for these other sources should not be affected by a large optical depth in the $H_2{}^{12}CO$ line.

For Sgr A the peak absorption percentage is 85 percent at a radial velocity of $+47$ km s^{-1}. The maximum absorption occurs near the edge of the source, so the peak value is somewhat uncertain, but we do not believe that the optical depth is much greater than 2. It can also be shown by using model fits to the absorption data that a formaldehyde distribution composed of one or two smaller-diameter clouds each of high optical depth is not compatible with our data. The clouds are definitely resolved. It is possible, however, that the clouds are composed of many small clumps.

The resulting $^{12}C/^{13}C$ isotopic ratio we obtain from Sgr A is 25 ± 5 (estimated standard error). This ratio reflects the real $^{12}C/^{13}C$ ratio if (1) the $H_2{}^{12}CO$ line is not saturated, (2) the two species of formaldehyde have the same excitation temperature and similar spatial distribution, (3) the production and destruction rate are the same for each, and (4) there are not many small clumps with higher optical depth.

Between radial velocities of $+55$ and $+67$ km s^{-1} the optical depth over part of Sgr B2 is large. The area within the 3.0 contour level (fig. 8) corresponds to an absorption greater than 95 percent. The optical depth, based solely on the data, could be infinite. In obtaining the value of NLT^{-1} for Sgr B2 shown in table 1, we have assumed a maximum optical depth of 3.0 corresponding to a 95 percent absorption in these opaque regions. Thus the value of NLT^{-1} is a lower limit.

The estimate of $^{12}C/^{13}C$ derived for Sgr B2 is greater than 20. The same restrictions apply as for Sgr A in interpreting the above value as the real abundance ratio of $^{12}C/^{13}C$ in the cloud. There is a possibility that the $H_2{}^{13}CO$ absorption is not optically thin.

An optical-depth effect in the $H_2{}^{12}CO$ line has already been suggested by Gardner, Ribes, and Cooper (1971). They found an intermediate value of 15 for the ratio

$^{12}C/^{13}C$ with a beam of 4'.3, intermediate between our resolution and 6'.6 of ZBPS.

The apparent isotopic ratio of $^{12}C/^{13}C$ corrected for $H_2{}^{12}CO$ saturation is about 25 in Sgr A and greater than 20 in Sgr B2. This value is still significantly less than the terrestrial value of 89. A ratio of 82 derived from optical studies of $^{13}CH^+$ (Bortolot and Thaddeus 1969) and recent $H_2{}^{13}CO$ measurements (Zuckerman *et al.* 1970*b*), giving the ratio 105 ± 30 for W33N, 63 ± 20 for W51, and greater than 84 for NGC 2024, suggest that there is an excess of the ^{13}C isotope in the galactic center region.

d) *The* 40 km s^{-1} *Cloud in Sagittarius A*

The projected density of $H_2{}^{12}CO$ in the 40 km s^{-1} feature of Sgr A is shown in figure 11. The velocity range of the cloud is +29 km s^{-1} to about +66 km s^{-1}. From figure 10 the absorption between +10 and +29 km s^{-1} usually included in this feature is located north of the galactic source and associated with a different cloud. A kink in the profile of the formaldehyde absorption near +25 km s^{-1} (see fig. 3*a* of ZBPS) also suggests the existence of another cloud.

The position and size of the cloud from other formaldehyde 4830-MHz observations (Kerr and Sandqvist 1970; ZBPS) agree well with our determination. Observations of OH absorption and CO emission leave little doubt that the distribution of these molecules is also similar to formaldehyde. A weak absorption line in H I at 40 km s^{-1} also has the same line width as the formaldehyde line when the absorption between +10 and +29 km s^{-1} is not included in the latter profile (Sandqvist 1970; Kerr and Vallak 1967). The hydrogen position and size have not been measured, but it is probably coincident with the cloud. The regions of the ammonia emission (Cheung *et al.* 1968) and 2-mm formaldehyde emission (Thaddeus *et al.* 1971) are south of the continuum source so that H_2CO absorption could not be detected there. However, the velocity of the emission regions agree with the expected velocity of the 40 km s^{-1} cloud in this region.

Based on the velocity structure, the cloud appears to be rotating as a solid body as first proposed by Kerr and Sandqvist (1968). If it is assumed that the cloud is 5' × 2'.5 with a rotational velocity of 20 km s^{-1} near the edge, that it is in gravitational equilibrium and at a distance of 10 kpc, we obtain a mass of the cloud of $\sim 3 \times 10^5\ M_\odot$. The estimated mass of atoms and molecules determined from absorption and emission measurements is much less than $10^3\ M_\odot$.

Assuming that the cloud is 10 pc in the line of sight (comparable with the transverse dimension) and that the missing mass is in the form of hydrogen molecules, a density of $\sim 10^5$ cm^{-3} is obtained for H_2. Such a density is indeed sufficient to excite OH and H I to the kinetic temperature. A much lower density was derived by Scoville, Solomon, and Thaddeus (1972), who also assumed that the cloud was rotating. The discrepancy is caused by the larger size they assigned to the cloud because of their lower resolution. However, the density of $\sim 10^5$ cm^{-3} is merely an estimated average. Variations in density are likely to occur within the cloud as suggested by the detection of 2-mm formaldehyde emission only in the southern part of the cloud.

There is some disagreement between the density of molecular hydrogen in the Sgr A cloud using the ratio of 2×10^{-9} for N_{H_2CO}/N_{H_2} found by Thaddeus *et al.* (1971) in Orion A and that determined from the gravitational stability of the Sgr A cloud which suggests a ratio of $\sim 3 \times 10^{-10}$. However, both determinations can be in error by an order of magnitude.

We thank J. Lequeux for suggesting this project and for useful comments on the manuscript. Research at the Owens Valley Radio Observatory is sponsored by the office of Naval Research under contract N00014-67-A-0094-0019 and by the National Science Foundation under contract GP25225.

REFERENCES

Bortolot, V. J., Jr., and Thaddeus, P. 1969, *Ap. J. (Letters)*, **155**, L17.
Cheung, A. C., Rank, D. M., Townes, C. H., Thornton, D. D., and Welch, W. J. 1968, *Phys. Rev. Letters*, **21**, 1701.
Fomalont, E. B. 1968, *Ap. J. Suppl.*, **15**, 203.
Fomalont, E. B., Wyndham, J. D., and Bartlett, J. F. 1967, *A.J.*, **72**, 445.
Gardner, F. F., Ribes, J. C., and Cooper, B. F. C. 1971, *Ap. Letters*, **9**, 181.
Kerr, F. J., and Sandqvist, A. 1968, *Ap. Letters*, **2**, 195.
———. 1970, *ibid.*, **5**, 59.
Kerr, F. J., and Vallak, R. 1967, *Australian J. Phys. Suppl.*, No. 3.
Palmer, P., Zuckerman, B., Buhl, B., and Snyder, L. E. 1969, *Ap. J. (Letters)*, **156**, L147.
Penzias, A. A., Jefferts, K. B., and Wilson, R. W. 1971, *Ap. J.*, **165**, 229.
Read, R. B. 1963, *Ap. J.*, **138**, 1.
Reifenstein, E. C., III, Wilson, T. L., Burke, B. F., Mezger, P. G., and Altenhoff, W. J. 1970, *Astr. and Ap.*, **4**, 357.
Rogstad, D. H., Rougoor, G. W., and Whiteoak, J. R. 1967, *Ap. J.*, **150**, 9.
Sandqvist, A. 1970, *A.J.*, **75**, 135.
Scoville, N. Z., Solomon, P. M., and Thaddeus, P. 1972, *Ap. J.*, **172**, 335.
Thaddeus, P. 1972, *Ap. J.*, **173**, 317.
Thaddeus, P., Wilson, R. W., Kutner, M., Penzias, A. A., and Jefferts, K. B. 1971, *Ap. J. (Letters)*, **168**, L59.
Townes, C. H., and Cheung, A. C. 1969, *Ap. J* . **157**, L103.
White, R. E. 1971, unpublished dissertation, Columbia University.
Whiteoak, J., and Gardner, F. F. 1970, *Ap. Letters*, **5**, 5.
Zuckerman, B., Buhl, D., Palmer, P., and Snyder, L. E. 1970*a*, *Ap. J.*, **160**, 485 (ZBPS).
Zuckerman, B., Palmer, P., Snyder, L. E., and Buhl, D. 1969, *Ap. J. (Letters)*, **157**, L167.
Zuckerman, B., Snyder, L. E., Palmer, P., and Buhl, D. 1970*b*, paper presented at the 132nd Meeting of the A.A.S., Boulder, Colorado, June 9–12.